STAT1 and STAT3 are expressed in the human ovary and have JAK1-independent functions in the COV434 human granulosa cell line

ER Frost[1,2,3,*], **EA Ford**[1,2], **AE Peters**[1,2], **NL Reed**[1], **EA McLaughlin**[1,4,5], **MA Baker**[1,2], **R Lovell-Badge**[3], **JM Sutherland**[1,2]

[1]Priority Research Centre for Reproductive Science, Schools of Biomedical Science & Pharmacy and Environmental & Life Sciences, University of Newcastle, Callaghan, New South Wales, Australia, 2308

[2]Hunter Medical Research Institute, New Lambton Heights, New South Wales, Australia, 2305

[3]Stem Cell Biology and Developmental Genetics Lab, The Francis Crick Institute, London, United Kingdom, NW1 1AT

[4]School of Science, Western Sydney University, Penrith, New South Wales, Australia, 2751

[5]School of Biological Sciences, Faculty of Science, University of Auckland, Auckland, New Zealand, 1142

Abstract

Ovarian granulosa cells are fundamental for oocyte maintenance and maturation. Recent studies have demonstrated the importance of members of the JAK/STAT signalling pathway in the granulosa cell population of mouse and horse ovaries, with perturbation of JAK1 signalling in mouse shown to impair oocyte maintenance and cause accelerated primordial follicle activation. The presence and role of the JAK/STAT pathway in human granulosa cells has yet to be elucidated. In this study, the expression of JAK1, STAT1 and STAT3 protein was detected in the oocytes and granulosa cells of human ovarian sections from foetal (40 weeks of gestation) and pre-menopausal ovaries (34 - 41 years of age) (N = 3). To determine the impact of JAK1 signalling, the human granulosa-like cell line, COV434 cells, was utilised with the JAK1 chemical inhibitor Ruxolitinib. Chemical inhibition treatment of COV434 cells with 100 nM of Ruxolitinib for 72 h, resulted in a significant increase in both *STAT3* mRNA ($p = 0.034$) and pY701STAT1 protein ($p = 0.0025$), demonstrating a role for JAK1 in modulating STAT in granulosa cells. This study implicates a conserved role for JAK/STAT signalling in human ovary development, warranting further investigation of this pathway in human granulosa cell function.

*Corresponding author: Emily Frost, Stem Cell Biology and Developmental Genetics Lab, The Francis Crick Institute, 1 Midland Road, London NW1 1AT, United Kingdom, Phone: +44 (0)20 3796 0000, emily.r.frost@uon.edu.au.

Conflict of Interest
The authors declare no conflicts of interest.

Introduction

Infertility affects approximately 12% of couples of reproductive-age (Inhorn and Patrizio 2015). In women, the intricate and dynamic nature of ovarian development makes infertility challenging to diagnose and treat effectively. Throughout development, the ovary is comprised of several cell types, including germ cells (oocytes) and the supporting somatic cells (granulosa and theca cells). While mature theca cells provide the components necessary for hormone synthesis in the post-natal ovary, granulosa cells develop alongside oocytes *in utero*. During gestation, pre-granulosa cells surround the diplotene oocyte and form primordial follicles (McLaughlin and McIver 2009; Ford *et al.* 2019). These follicles remain quiescent and form the ovarian reserve; the store from which all oocytes mature, which sustains fertility throughout a woman's reproductive lifespan (Kallen *et al.* 2018). From this stage on, the granulosa cells remain in constant contact with the oocyte, either directly to the oocyte surface, or through transzonal processes that extend through the zona pellucida and attach to gap junctions on the oocyte membrane (Eppig 2018). This direct contact is essential to maintaining the meiotic quiescence of the oocyte, a requirement of pre-ovulatory follicle development (Norris *et al.* 2008).

Cross-talk from the granulosa cells is essential to the formation of a healthy oocyte, competent for fertilisation. A number of recent studies have highlighted the importance of granulosa cell function in oocyte maturation. In 2018, El-Hayek and colleagues demonstrated that the greater the number of granulosa cells in contact with the oocyte, the faster the oocyte is able to grow (El-Hayek *et al.* 2018). These granulosa cells supplement the oocyte with essential metabolic compounds required for their rapid growth (El-Hayek *et al.* 2018). Similarly, it has been demonstrated using a cyclophosphamide-induced mouse infertility model, that poor-quality granulosa cells reduce follicle quality (Xiong *et al.* 2017). Dissociated granulosa cells of cyclophosphamide-treated mice were unable to proliferate and entered senescence *in vitro. In vivo,* granulosa cells had high levels of p53 and cleaved caspase 3, contributing to the infertility phenotype of the mice (Xiong *et al.* 2017). Furthermore, in mice it has been demonstrated, using RNA-sequencing and gene deletion experiments, that granulosa cells utilise gap junctions to initiate crucial signalling events with the oocyte through the secretion of cytokines, such as KITL/KIT and the transferral of transcription factors (Zhang *et al.* 2014; Bonnet *et al.* 2015).

With the advent of *in vitro* fertilisation (IVF), many studies have identified important roles for granulosa cells after their release from the ovary with the egg during ovulation. However, our understanding of granulosa cell function within the human ovary remains limited. It has been shown that granulosa cells in other mammals have multiple roles, including maintaining cell fate and specifying theca cell differentiation, in parallel with aiding egg maturation (reviewed in (Rotgers *et al.* 2018)). It is difficult to examine these functions in humans, due to the unavailability of healthy ovarian tissue from young donors. Human

granulosa cell lines present a valuable alternative to investigate the signalling molecules and pathways important to cellular proliferation within the developing follicles. Here we utilise the COV434 human granulosa cell line, as it recapitulates properties that are observed in primary human granulosa cells (Zhang *et al.* 2000). In particular, COV434 cells are diploid, grow in small aggregates, form gap junctions when co-cultured with cumulus-oocyte complexes and display markers of apoptosis which are also present during follicular atresia in human granulosa cells (van den Berg-Bakker *et al.* 1993; Zhang *et al.* 2000). These properties of the COV434 cell line make it a suitable model for examining granulosa cell signalling pathways and interactions in the human ovary.

The JAK/STAT pathway is a well-understood cell proliferation pathway in many organs. Transcriptomic analyses of human follicles identified high abundance of *STAT3* mRNA in early-stage follicles (Ernst *et al.* 2018b). Recent findings have demonstrated a key role for the JAK/STAT signalling pathway in the regulation of all stages of follicle development in the mouse and horse (Sutherland *et al.* 2012; Hall *et al.* 2017; Sutherland *et al.* 2018). The objective of the current study was to determine if selective JAK/STAT members were present in the granulosa cells of human ovarian tissue sections and to use the COV434 human granulosa cell line to examine changes in the JAK1 pathway with inhibition. To this end, we investigated the expression of JAK1, STAT1 and STAT3 in human ovarian tissue sections, both embryonically and in adulthood. JAK1, STAT1 and STAT3 were all expressed in granulosa cells, specifically in primordial follicles, indicating the JAK/STAT pathway as a conserved signalling pathway interacting in granulosa cell functions in mammals. Functional analysis using the COV434 cell line demonstrated that the JAK1 inhibitor, Ruxolitinib, increased the expression of *STAT3* mRNA in COV434 cells and increased STAT1 activation. This demonstrates a role for JAK1 in modulating STAT proteins in granulosa cells. Taken together, our findings demonstrate the presence of JAK/STAT signalling in human ovarian follicles and present a novel role for this pathway in human granulosa cell function.

Materials and Methods

Ethical Approval

All studies were performed in accordance with the University of Newcastle's Human Ethics Committee guidelines (Approval no. H – 2016-0441). Normal human foetal ovary sections (40 weeks of gestation) were obtained from Abcam (#ab4412). Human pre-menopausal ovary sections were supplied by the Hunter Cancer Biobank. Pre-menopausal non-cancerous human ovaries were removed from patients between 34 and 41 years of age, with oral and written consent. All ovary samples that were used were confirmed as histologically normal by pathologists.

Immunofluorescence on human ovary sections

Sections were received from the Hunter Cancer Biobank and were subjected to a series of xylene and ethanol washes. Heat-mediated antigen retrieval was performed on the slides using either 10 mM sodium citrate buffer (pH 6) or 10 mM TRIS buffer (pH 8) for 25 minutes. After blocking, the following primary antibodies were used for immunofluorescence: JAK1 (ab47435 Abcam), STAT1 (ab2415 Abcam) and STAT3 (79D7

Cell Signalling Technologies). Goat-anti-rabbit Alexa 555 secondary antibody (ab150078, Life Technologies) was used at a concentration of 20 μg/mL for visualisation of the primary antibodies. After counter-staining with 4'-6-diamidino-2-phenylindole (DAPI) and mounting in Mowiol (13% Mowiol4-88, 33% glycerol, 66 mM Tris (pH 8.5), 2.5% 1,4 diazobcyclo-[2.2.2]octane), the sections were imaged using an Axio Imager A1 fluorescent microscope (Carl Zeiss MicroImaging, Inc, Thornwood, NY). Images were taken using an Olympus DP70 microscope camera (Olympus America, Center Valley, PA) and post-image analysis was done using the fluorescence microscope software Zen (Carl Zeiss Ltd., Thornwood, NY). The stages of follicular development within the human ovarian tissue sections were determined according to the criteria outlined by Gougeon (Gougeon 1996). Images for all 3 biological replicates of JAK1, STAT1 and STAT3 proteins in human foetal and pre-menopausal ovarian tissues are shown in Supplementary Figures 1 and 2.

Cell culture

COV434 cells are an immortalised human granulosa carcinoma cell line, derived from a solid tumour of a 27-year-old female patient. COV434 cells were supplied through Sigma from the European Collection of Authenticated Cell Cultures (ECACC) and were thawed from frozen stocks. The cells were cultured in 1x Low Glucose Dulbecco's Modified Eagle Medium (DMEM-low glucose, Sigma, Missouri, USA) with 10% foetal bovine serum (FBS) and 1% penicillin/streptomycin (PS, Thermofisher, Madison, USA) at 37 °C in 5% CO_2. The medium was changed every four days, and the cells were passaged once a week.

Inhibitor treatment

The commercially available inhibitor Ruxolitinib (CAS 941678-49-5, Santa Cruz, Dallas, USA) was used for inhibition of JAK1 signalling in COV434 cells. The manufacturer's mechanism of action for Ruxolitinib, involves competitive binding to the JAK1 receptor, disabling JAK phosphorylation and preventing downstream signalling to STAT proteins. The appropriate inhibitor concentrations and treatment length were based on the IC50 of Ruxolitinib and were optimised specifically for COV434 cells (data shown in Supplementary Figure 4). Cells were treated for 72 hr as COV434 cells are slow-growing and require time to cell cycle for proliferation effects to be examined (Pastuschek *et al*. 2015). This treatment length also demonstrated the most robust decrease in JAK1 phosphorylation, compared with 24 hr and 48 hr treatments (data not shown). COV434 cells to be treated with Ruxolitinib for collection were plated at a density of 400,000 cells/well in 6-well plates and grown overnight. The next day, 4 mL of media containing 100 nM Ruxolitinib was added to the cells, and cells were treated for 72 hr. Following treatment, the cells were counted and were either centrifuged into cell pellets for RNA or protein extraction or fixed using paraformaldehyde and spotted onto glass slides for immunocytochemistry (ICC).

Cell fixation

COV434 cells following growth or treatment were trypsinised and washed in PBS to make a 1 million cells/mL solution and transferred to a 1.5 mL tube. The cells were centrifuged and 4% paraformaldehyde (PFA) was added to the tube. The cell pellet was re-suspended in the PFA and placed on the rotator for 15 minutes at room temperature. After washing in PBS,

the cells were re-suspended in PBS and 10 μL of cell suspension was spotted on each well on 12-well frosted slides (Thermofisher, Madison, USA) and stored at -20 °C until ICC was performed.

CCK-8 analysis

Cell proliferation was measured using a Cell Counting Kit-8 (CCK-8) assay (Sigma, Missouri, USA). COV434 cells to be treated for CCK-8 analysis were plated at a density of 10,000 cells/well in 96-well plates and left to grow overnight. The cells were treated with DMSO or Ruxolitinib for 48 hours, and CCK-8 reagent was added to each well and incubated for 2 hours in standard culture conditions. The absorbance reading at 450 nm was taken for each sample, using a microplate imaging system (Biorad, CA, USA). All results obtained after Ruxolitinib treatments were compared with those obtained using dimethyl sulfoxide (DMSO) as a vehicle control and normalised against media only control readings.

RNA extraction and cDNA synthesis

Total RNA was extracted from COV434 cell pellets (2×10^6 cells per pellet) using an RNeasy-Mini Kit (Qiagen, Venlo, Netherlands). The cells were homogenised using a pestle and a 20 G needle. The sample was left on ice for 10 minutes before the total RNA was extracted from COV434 cell pellets according to the manufacturer's instructions (Qiagen, Venlo, Netherlands). Following extraction, RNA concentration and sample purity were calculated using a spectrophotometer. Reverse transcription was performed on each sample with 2 μg of isolated RNA, 1 μL of oligo-dTs, 4 μL of 5x buffer, 2 μL DTT, 1 μL RNasin, 1 μL 10mM dNTPs and 1 μL of M-MLV-reverse transcription (RT) enzyme (Promega, Madison, USA). Samples were pipette mixed and pulse spun 3 times and then incubated at 42 °C for 2 hours. The samples were then incubated at 70 °C for 10 minutes to inactivate the enzyme, and then 80 μL of nuclease-free H_2O was added to each tube. The presence of cDNA was confirmed using standard PCR using ribosomal protein L19 (*RPL19*) primers and RT samples were stored at -20 °C.

Quantitative PCR (qPCR)

Quantitative PCR was performed on the COV434 cell cDNA, using SYBR Green GoTaq qPCR Master Mix according to the manufacturer's instructions (Promega, Madison, USA). cDNA equivalent to 100 ng of total RNA was used for each reaction, for 40 amplification cycles on the Roche Light Cycler 96 machine (Roche, Basel, Switzerland). For each sample, a replicate omitting the reverse transcription enzyme was utilised as a negative control. Specific primer sequences and annealing temperatures for each gene are available as supplementary data (Supplementary Table 1). All primers were tested using gradient temperatures and cDNA dilutions for efficiency values. Quantitative PCR data were analysed using the Light Cycler program, and the equation $2^{-\Delta CT}$, where CT is the cycle that fluorescence was first detected above background fluorescence. Data were normalised to *B-ACTIN* and is presented as the mean ± SEM expression of each target gene, relative to the mean of *B-ACTIN* expression. *B-ACTIN* was chosen as the appropriate house-keeping gene as it maintained expression levels between control and treatment groups, and was more stable than *GAPDH, HPRT1* and *PPIA*. This comparison was performed using the

NormFinder software (Andersen *et al.* 2004) and the data is shown in Supplementary Figure 3.

Protein extraction and immunoblot

Protein was extracted from 2×10^6 COV434 cells using 150 μL of RIPA extraction buffer (150 mM sodium chloride, 0.5% sodium deoxycholate, 0.1% SDS, Protease/phosphatase inhibitor cocktail 100x). The BCA Protein Assay Kit (Thermo Scientific, Walthman, MA) was used to quantify the total extracted protein in the sample. Immunodetection was conducted using the following primary antibodies: JAK1 (1:1000 dilution, ab133666, Abcam), pJAK1 (1:1000 dilution, #3331, Cell Signalling Technologies), JAK2 (1:1000, ab ab68273, Abcam), STAT1 (1:1000, #9172, Cell Signalling Technologies), pSTAT1 (1:1000, 333400, Thermofisher), STAT3 (1:1000, 79D7, Cell Signalling Technologies) and pSTAT3 (1:1000, ab76315, Abcam). The next day following washing, the blot was incubated with either a goat-anti-rabbit HRP-conjugated secondary antibody (ab205718, Abcam) or a rabbit-anti-mouse (ab6728, Abcam) at a 1:1000 dilution for 2 hours at RT. Labelled antibodies were detected using an Amersham ECL Detection Kit (GE Healthcare UK Limited, Buckinghamshire, UK). GAPDH (G9545, Sigma–Aldrich) was used as a loading control. Densitometry was performed using the Amersham Imager 600 software (GE Healthcare). The protein expression was normalised to GAPDH and presented as the mean ± SEM expression of each target protein, relative to GAPDH.

Immunocytochemistry (ICC)

COV434 cell slides were prepared and probed with antibodies specific for JAK1 (ab47435, Abcam), pJAK1 (ab138005, Abcam), STAT1 (ab2415, Abcam) and STAT3 (79D7, Cell Signalling Technologies). Primary antibodies were visualised using either a goat-anti-rabbit Alexa 555 secondary antibody (ab150078, Life Technologies) or a goat-anti-mouse Alexa 555 secondary antibody (a21422, Life Technologies) at a 1:100 dilution and 4′-6-Diamidino-2-phenylindole (DAPI) was used as a nuclear counterstain. Slides were imaged using the Axio Imager A1 fluorescent microscope (Carl Zeiss MicroImaging, Inc, Thornwood, NY) and Olympus DP70 microscope camera (Olympus America, Center Valley, PA).

Statistical analyses

All statistical analyses were performed using GraphPad Prism (version 7, GraphPad Software, CA, USA). Data with less than three groups were analysed using the independent samples T-test for parametric data. Data with more than two groups were analysed using two-way analysis of variance (ANOVA). Datasets that showed a skewed distribution, either positive or negative, were analysed using non-parametric Wilcoxon/Kruskal-Wallis testing. Unless otherwise stated, all data is presented as mean ± standard error of the mean (SEM). Statistical significance was considered as $p < 0.05$. In figures, an asterisk(s) denotes statistical significance (*$p < 0.05$, **$p < 0.01$ and ***$p < 0.001$). All experiments were performed in biological triplicate unless otherwise stated.

Results

JAK1, STAT1 and STAT3 are expressed in human foetal and pre-menopausal ovaries

To determine whether the JAK/STAT signalling pathway was indeed active in the human ovary, immunofluorescence was utilised to assess the protein localisation of the candidate members JAK1, STAT1 and STAT3 on foetal (40 weeks of gestation) and pre-menopausal (34 – 41 years old) human ovary sections. These three candidate JAK/STAT pathway members are known to be expressed in the granulosa cells of neonatal and adult mouse ovary (Sutherland *et al.* 2012; Sobinoff *et al.* 2013; Sutherland *et al.* 2018). Moreover, all three candidates have also been shown to functionally interact in multiple tissues including ovary (Sutherland *et al.* 2012; Sobinoff *et al.* 2013; Sakamoto *et al.* 2016; Liang *et al.* 2017).

Within the foetal human ovary, JAK1 protein was primarily localised to the oocytes of newly formed primordial follicles (Figure 1*a* , denoted by white asterisk). Faint JAK1 expression was also detected in the connecting stromal tissue, and surrounding interstitial cells (Figure 1*a* , identified by green arrow). Interestingly, JAK1 expression was noticeably absent from the surrounding pre-granulosa cells of primordial follicles (Figure 1*a* , primordial follicles identified by asterisks, granulosa cells identified by white arrows). Similar to JAK1, both STAT1 and STAT3 localised to the primordial oocytes of the foetal ovary (Figure 1*b* and 1*c* , denoted by white asterisk). This expression manifested as distinct foci, shown by the intense pixels observed in the oocyte nucleus and cytoplasm (Figure 1*b* and 1*c* , denoted by white circles). Faint expression of STAT1 and STAT3 was detected in the granulosa cells of primordial and primary follicles (Figure 1*b* and 1*c* , denoted by white arrows).

In the adult pre-menopausal ovary, JAK1 protein expression was detected in the oocyte and pre-granulosa cells of primordial follicles (Figure 2*a* , oocyte shown by white asterisk and pre-granulosa cells shown by white arrow). In primary follicles, JAK remained localised to the granulosa cells of the follicle, however, JAK1 oocyte expression was undetectable (Figure 2*a* , oocyte indicated by white asterisk and granulosa cells indicated by white arrow). STAT1 expression in the adult pre-menopausal ovary was consistent with the expression seen in the foetal ovary. STAT1 protein was observed in the oocyte and granulosa cells of primordial and primary follicles (Figure 2*b* , oocyte shown by white asterisk and granulosa cells shown by white arrow). Aggregates of STAT1 protein were localised in the nucleus of the oocyte in both primordial and primary follicles (Figure 2*b* , shown circled in white). In the adult ovary, STAT3 localised largely to the granulosa cells of primordial and primary follicles (Figure 2*c*), with only faint STAT3 expression detected in the cytoplasm of oocytes (Figure 2*c* , denoted by white asterisk). These data indicate a role for pivotal JAK/STAT pathway members, JAK1, STAT1 and STAT3, in early follicle development, warranting further investigation of these proteins in human granulosa cells.

JAK1, STAT1 and STAT3 are expressed in the human granulosa-like COV434 cell line

Due to the limitations of models to study early-stage human follicles, the COV434 human granulosa cell line was utilised. While this cell line is not representative of granulosa cells from primordial or primary follicles, it does allow the study of signalling dynamics to incorporate functional analyses and manipulation of the JAK/STAT pathway. The COV434

human granulosa cell line was chosen as an appropriate model as they recapitulate the properties observed in primary human granulosa cells (Zhang *et al.* 2000). Preliminary investigations to validate JAK1, STAT1 and STAT3 expression in COV434 cells were performed using quantitative PCR (qPCR), immunoblotting and immunolocalisation approaches.

All three candidates (*JAK1, STAT1* and *STAT3*) were detected at the mRNA level in the COV434 cells and demonstrated comparable mRNA abundance as measured by qPCR relative to the steady-state housekeeping gene (*B-ACTIN*) (Figure 3*a*). Subsequent immunoblot analysis validated that JAK1, STAT1 and STAT3 proteins were indeed expressed within the COV434 cells (Figure 3*b*). Densitometric analysis determined that these proteins were also expressed at similar levels, relative to GAPDH (Figure 3*c*).

Having confirmed the presence of the JAK1, STAT1 and STAT3 mRNA and protein in COV434 cells, we next sought to determine the subcellular localisation of these proteins via immunocytochemistry. JAK1 localised to both the cytoplasm and the nucleus of COV434 cells, with intense staining specifically in the nucleus (Figure 4*a*, identified by white arrows). In a similar fashion to JAK1, STAT1 and STAT3 both demonstrated nuclear and cytoplasmic protein expression, however, the intensity of the signal was variable between cells indicating the heterogeneity of the sample (Figure 4*b* and Figure 4*c*, cytoplasm identified by green arrows). A summary table of JAK1, STAT1 and STAT3 expression can be found in Supplementary Table 2. This experiment identified that the same members of the JAK/STAT family, namely JAK1, STAT1 and STAT3, were expressed in both the human ovarian sections and the COV434 cells. Having validated the conserved expression of the pathway, subsequent investigations were undertaken using this cell line to gain a mechanistic understanding of the importance of the upstream regulator JAK1 on cellular activities.

JAK1 is inhibited by the chemical inhibitor Ruxolitinib in COV434 cells

To modulate the JAK/STAT pathway in COV434 cells, we employed an *in vitro* biochemical inhibition approach to limit the action of JAK1, as the upstream regulator. To this end, we utilised the established pan JAK1/2 inhibitor, Ruxolitinib, to disrupt cellular signalling. COV434 cells were treated with either a vehicle control (DMSO) or increasing doses of Ruxolitinib for 72 hours and collected for assessment. 100 nM of Ruxolitinib was determined as the lowest concentration of Ruxolitinib that inhibited the activation of JAK1, as measured by immunocytochemistry, while not inducing apoptosis, as measured by decreased cell number, and was consequently selected for use in all subsequent experiments (Supplementary Figure 4). To establish the phenotype of granulosa cells treated with 100 nM Ruxolitinib, post-treatment live cell counts and proliferation analysis using Cell Counting Kit-8 (CCK-8) were performed. There was no effect observed in COV434 cells subjected to Ruxolitinib treatment, in terms of total (live) cell number or cell proliferation rates, when compared to the vehicle only control (Figure 5*a* and 5*b*).

To confirm the inhibition of JAK1 activity and verify the targets of Ruxolitinib, immunoblotting was conducted for JAK1, pY1034/35JAK1 and JAK2. A visible decrease in total JAK1 and phosphorylated JAK1 were observed at the 100 nM Ruxolitinib dose in COV434 cells and supported by immunocytochemistry (Supplementary Figure 5).

Importantly, there was no significant difference in JAK2 expression following Ruxolitinib treatment, indicating that the subsequent downstream pathway members are affected as a direct result of JAK1 modulation (Figure 6).

STAT1 and STAT3 function downstream of JAK1 inhibition in COV434 cells

Having established the 72 h 100 nM Ruxolitinib treatment regime as an appropriate approach to directly inhibit JAK1, quantitative PCR (qPCR) was performed for the downstream candidates *STAT1* and *STAT3* on treated COV434 cells. No significant decreases in mRNA abundance were observed for *STAT1* (Figure 7*a*). Interestingly, *STAT3* mRNA expression increased with Ruxolitinib treatment (p = 0.034) (Figure 7*b*).

We extended our examination of the impact of cell treatment by conducting immunoblotting on COV434 cell total protein lysates. No significant differences in total protein expression were observed for STAT1 or STAT3 (Figure 8*a* and 8*b*). To determine the impact of Ruxolitinib inhibition on STAT1 and STAT3 activation via tyrosine phosphorylation, immunoblot analysis for phosphorylated Y701 STAT1 (pSTAT1) and phosphorylated Y705 STAT3 (pSTAT3) was conducted. A significant increase was observed in pSTAT1 protein as a result of Ruxolitinib treatment (p = 0.0025) (Figure 8*c*). Ruxolitinib treatment did not appear to affect (NS) pSTAT3 levels (Figure 8*d*). These results suggest that Ruxolitinib inhibition of JAK1 primarily effects the activation of STAT1 with no effect on STAT3 protein in the COV434 human granulosa cell line.

Discussion

It is well established that oocyte-granulosa cell signalling interactions facilitate and encourage proper maturation events at specific temporal windows (McLaughlin and McIver 2009; Hsueh *et al.* 2015; Ford *et al.* 2019). Granulosa cells must provide the oocyte with a variety of metabolites and substrates throughout oocyte maturation (Laissue *et al.* 2008; Shelling 2010). In multiple species, the JAK/STAT pathway has been identified in oocyte and granulosa cells (Anderson *et al.* 2009; Sutherland *et al.* 2012; Monahan and Starz-Gaiano 2013; Sobinoff *et al.* 2013; Yang and Fortune 2015; Hall *et al.* 2017; Sutherland *et al.* 2018). In this study, we have established the JAK/STAT pathway in the human ovary. We identified JAK1, STAT1 and STAT3 protein expression in both the human foetal and premenopausal ovary. The expression of JAK1 validates a single-cell RNA sequencing study that identified the upregulation of JAK1 in human primary follicles (Zhang *et al.* 2018). The pattern of foci within the nucleus of the oocyte for STAT1 and STAT3 is consistent with the mechanism of action of STATs, where they dimerise and bind to target genes to promote gene upregulation (Kisseleva *et al.* 2002). Our results are consistent with the recent large-scale RNA profiling of human primordial follicles, which showed enrichment of *STAT3* transcript (Ernst *et al.* 2018a). We focused our investigations on the function of the JAK1, STAT1 and STAT3 cascade in human granulosa cells. This required the use of a human granulosa cell model, the COV434 cell line.

The COV434 cell line is responsive to LIF treatment, which is known to upregulate JAK1 and STAT3 specifically (Pastuschek *et al.* 2015). We found that JAK1, STAT1 and STAT3 proteins were all localised to the nucleus and cytoplasm of COV434 cells in a heterogeneous

manner. While conventional roles for the JAK proteins are cytoplasmic, there is increasing evidence to suggest that JAK proteins uncouple from their transmembrane receptor and become imported into the nucleus (Lobie *et al.* 1994; Gual *et al.* 1998; Zouein *et al.* 2011). This reveals multiple roles for JAK proteins, including binding to and regulating the expression of other target genes within the nucleus. While in this study, we observed no changes in JAK1 localisation with Ruxolitinib treatment, further studies identifying binding partners of JAK1 or the binding of JAK1 to DNA would further decipher JAK1 actions.

Using the COV434 cell line also allowed for the functional modulation of the JAK/STAT pathway. Having established that JAK1 is present in COV434 cells, we performed *in vitro* inhibition assays to examine the functional role of JAK1. This was achieved by using the JAK inhibitor Ruxolitinib (Quintas-Cardama *et al.* 2010). Ruxolitinib is a pan JAK1/JAK2 inhibitor, used in the treatment of myelofibrosis, to inhibit the JAK/STAT pathway and prevent the proliferation of cancerous cells (Shaker *et al.* 2016; Gowin *et al.* 2017; Verstovsek *et al.* 2017). We optimised treatment of COV434 cells with varying doses of Ruxolitinib, finding 100 nM Ruxolitinib the optimal treatment dose for decreasing JAK1 activity without causing cell death. The decrease in JAK1 activity was seen in the observable decrease in phosphorylated JAK1. We did not see a significant difference in total JAK1 protein, and we hypothesise that this is due to the mechanism of the action of Ruxolitinib. The manufacturers report that Ruxolitinib acts through JAK1 inactivation, rather than JAK1 degradation. This compound binds to the JAK1 protein located on the receptor, preventing phosphorylation. In contrast to our previous findings in the mouse ovary (Sutherland *et al.* 2018), we observed that no changes in cell number or proliferation were seen with 100 nM Ruxolitinib treatment when compared to the vehicle control. This suggests that JAK1 may not play a role in regulating granulosa cell proliferation as predicted. One alternative role for JAK1 within the human granulosa cells may be as a nuclear regulator of other signalling cascades promoting proliferation, such as the PI3K pathway. In the mammary gland, cross-talk between PI3K activation and JAK/STAT signalling is established (Radler *et al.* 2017). A second option is that the JAK/STAT pathway remains more critical for communication events between the oocyte and surrounding granulosa cells as opposed to solely in granulosa cell proliferation. Mouse studies to conditionally delete JAK1 in granulosa cells *in vivo* or the culture of oocytes with JAK1-deficient foetal granulosa cells *in vitro* may uncover the intracellular mechanisms of JAK1.

Besides JAK1, other JAK family members have regulatory roles in establishing the follicle pool in mice, and so redundancy between the JAK family members may be observed in ovarian follicles (Huang *et al.* 2018). JAK1, JAK2 and TYK2 share homology in their JAK insertion loops and GQM binding domain, which may allow their promiscuity in binding to multiple receptors (Babon and Nicola 2012). Ruxolitinib is reported to bind to JAK2, with decreased efficacy, and has a greater than 130-fold selectivity for JAK1 and JAK2 versus JAK3 (Quintas-Cardama *et al.* 2010). We have little evidence to suggest that a JAK2 mechanism is occurring in our Ruxolitinib-treated COV434 cells. Western blotting confirmed that JAK1 is highly expressed in COV434 cells and is the principal JAK family member targeted by Ruxolitinib in the COV434 cells. Our data suggest that JAK2 is lowly expressed and not affected by Ruxolitinib-treatment, indicating a direct link between JAK1 and the downstream STAT members investigated.

Intriguingly, analysis of JAK1-inhibited COV434 cells revealed no significant changes in total protein for STAT1 and STAT3, while at the gene level, *STAT3* mRNA was significantly increased following Ruxolitinib-treatment (Figure 9). Two papers have previously shown STAT3 expression in human granulosa cells, both in the transcriptome and proteome (Pastuschek *et al.* 2015; Ernst *et al.* 2018b). As STAT3 has been shown in the mouse ovary to be a direct target of JAK1 (Sutherland *et al.* 2012), we hypothesised that inhibition of JAK1 results in a decreased phosphorylation of STAT3, thus effectively switching off the JAK1/STAT3 signalling cascade. However, when we examined phosphorylated STAT1 and STAT3 in Ruxolitinib-treated COV434 cells, we saw no change in activated STAT3 protein. This may be due to the Ruxolitinib treatment time, where compensatory mechanisms and alternate signals are re-establishing STAT3 activation in the absence of the JAK1 activating signal. Although JAK1 is considered a key modulator of STAT3, STAT3 is a target of other epigenetic regulators, including PI3K (Bian *et al.* 2018). This compensation could explain the increase in the transcription of *STAT3* transcript. Future experiments examining compensatory pathways including PI3K and ERK signalling, using live-cell imaging of GFP-tagged STAT3 protein (Cimica and Reich 2013; Khan *et al.* 2013), inhibition of nuclear export by inhibiting the CRM1 exportin (Cheng *et al.* 2014) or a change in treatment time may be more reflective of the dynamic pathway changes.

The family of STAT proteins are responsible for target gene activation by binding to the DNA and inducing gene expression. This action relies on stimulation of upstream proteins, like JAK1, to phosphorylate STATs and form homodimers to enter the cell nucleus (Hirahara *et al.* 2015). It is well known that functional redundancy exists in the activation of STAT signalling, particularly for STAT1 and STAT3 (Hirahara *et al.* 2015). JAK1 is described to stimulate cellular proliferation through the activation of STAT3 in numerous biological and pathological niches, including in the haematopoietic stem cells, astrocytes and gastric and colon carcinomas (Wei *et al.* 2013; Ceyzeriat *et al.* 2016; Kuepper *et al.* 2019; Wang *et al.* 2019). Direct interactions between JAK1 and STAT1 have also been identified in colon cancer and immune system regulation (Jia *et al.* 2017; Liang *et al.* 2017; Peng *et al.* 2018). In the context of COV434 cells, our results show a robust increase in activated STAT1 protein with 100nM Ruxolitinib treatment (Figure 8). In mouse embryonic fibroblasts, this phosphorylation at the same tyrosine residue Y701 of STAT1 results in the shuttling of STAT1 homodimers and STAT1 complexes to the nucleus (Sadzak *et al.* 2008). This suggests that with Ruxolitinib treatment, increased numbers of STAT1 homodimers are shuttled to the nucleus and initiate target gene expression. It is unclear what the consequences for the cells are, following this altered cell signalling, as we did not see an increase in proliferation or cell death (Figure 5). In human fibroblasts, increased levels of pSTAT1 are associated with increased levels of apoptosis, due to the activity of caspases (Kumar *et al.* 1997). Caspase activity has not previously been established in the COV434 cell model, but would provide insights into the functional importance of pSTAT1 upregulation. Increased amounts of pSTAT1 may also cause the recruitment of repressor complexes binding to the DNA. Future studies using ATAC-seq on Ruxolitinib treated COV434 cells would identify changes in activator or repressor functions on specific genes. Further work to untangle the mechanism, consequences and downstream targets of pSTAT1 could yield deeper insights into granulosa cell signalling.

Based on our inhibition data, we hypothesise that in the COV434 cells, STAT1 is activated by a compensatory pathway upon the loss of JAK1 activation. Both STAT1 and STAT3 are reported to be activated by JAK-independent mechanisms (Bousoik and Montazeri Aliabadi 2018). These STATs also share homology and target genes of STAT3 can be transcribed by activated STAT1 in *Stat3*$^{-/-}$ MEFs (Schiavone *et al.* 2011). However, this does not necessarily reflect the capacity of STAT1 to compensate for all STAT3 actions and transcription targets in granulosa cells. Further studies, such as ChIP-Seq, examining the DNA binding sites of STAT1 and ChIP-Proteomics to find protein binding partners, will elucidate whether the activation of STAT1 is regulated by the Ruxolitinib treatment or by other complementary pathways. Future experiments to investigate the expression of known STAT1 transcriptional targets in somatic cells, such as BCL2 (Sanda *et al.* 2013), p27 (Wang *et al.* 2008; Wang *et al.* 2010) and SOCS1 (Chan *et al.* 2014) would be of significant benefit in determining the cellular consequences of increased STAT1 phosphorylation on gene regulation. In particular, these targets have defined cellular roles. BCL2 is well-characterised as an anti-apoptotic factor, that tightly regulates the cell's intrinsic apoptosis pathway (Cui and Placzek 2018). Coupled with p27's role as a cell cycle inhibitor, that is established in the granulosa cells of the mouse ovary (Rajareddy *et al.* 2007), we hypothesise that changes in these factors may contribute towards altering the balance between proliferation and apoptosis, causing dysregulated COV434 cell cytokine release and growth signalling.

This study has provided evidence for responsive JAK/STAT signalling within human granulosa cells, which contributes to oocyte-granulosa cell crosstalk. We have found that STAT1 and STAT3 are activated by JAK1, and regulate the expression of important genes for granulosa cell communication. Interactions with other signalling pathways and regulators provide the mechanistic pathway of JAK/STAT signalling in granulosa cells, and future studies may untangle the complexity of cell function at the various stages of folliculogenesis. Understanding the spatial and temporal control that granulosa cells provide will lead to a better understanding of oocyte maturation and ultimately female fertility.

Supplementary Material

Refer to Web version on PubMed Central for supplementary material.

Acknowledgements

References

Andersen CL, Jensen JL, Orntoft TF. Normalization of real-time quantitative reverse transcription-PCR data: a model-based variance estimation approach to identify genes suited for normalization, applied to bladder and colon cancer data sets. Cancer Res. 2004; 64(15):5245–50. [PubMed: 15289330]

Anderson ST, Isa NN, Barclay JL, Waters MJ, Curlewis JD. Maximal expression of suppressors of cytokine signaling in the rat ovary occurs in late pregnancy. Reproduction. 2009; 138(3):537–44. [PubMed: 19502454]

Babon JJ, Nicola NA. The biology and mechanism of action of suppressor of cytokine signaling 3. Growth Factors. 2012; 30(4):207–19. [PubMed: 22574771]

Bian C, Liu Z, Li D, Zhen L. PI3K/AKT inhibition induces compensatory activation of the MET/STAT3 pathway in non-small cell lung cancer. Oncol Lett. 2018; 15(6):9655–9662. [PubMed: 29928341]

Bonnet A, Servin B, Mulsant P, Mandon-Pepin B. Spatio-Temporal Gene Expression Profiling during In Vivo Early Ovarian Folliculogenesis: Integrated Transcriptomic Study and Molecular Signature of Early Follicular Growth. PLoS One. 2015; 10(11):e0141482. [PubMed: 26540452]

Bousoik E, Montazeri Aliabadi H. "Do We Know Jack" About JAK? A Closer Look at JAK/STAT Signaling Pathway. Frontiers in Oncology. 2018; 8(287)

Ceyzeriat K, Abjean L, Carrillo-de Sauvage MA, Ben Haim L, Escartin C. The complex STATes of astrocyte reactivity: How are they controlled by the JAK-STAT3 pathway? Neuroscience. 2016; 330:205–205. [PubMed: 27241943]

Chan SR, Rickert CG, Vermi W, Sheehan KCF, Arthur C, Allen JA, White JM, Archambault J, Lonardi S, McDevitt TM, Bhattacharya D, et al. Dysregulated STAT1-SOCS1 control of JAK2 promotes mammary luminal progenitor cell survival and drives ERα(+) tumorigenesis. Cell death and differentiation. 2014; 21(2):234–246. [PubMed: 24037089]

Cheng Y, Holloway MP, Nguyen K, McCauley D, Landesman Y, Kauffman MG, Shacham S, Altura RA. XPO1 (CRM1) inhibition represses STAT3 activation to drive a survivin-dependent oncogenic switch in triple-negative breast cancer. Mol Cancer Ther. 2014; 13(3):675–86. [PubMed: 24431073]

Cimica V, Reich NC. Nuclear trafficking of STAT proteins visualized by live cell imaging. Methods Mol Biol. 2013; 967:189–189. [PubMed: 23296731]

Cui J, Placzek WJ. Post-Transcriptional Regulation of Anti-Apoptotic BCL2 Family Members. International journal of molecular sciences. 2018; 19(1):308.

El-Hayek S, Yang Q, Abbassi L, FitzHarris G, Clarke HJ. Mammalian Oocytes Locally Remodel Follicular Architecture to Provide the Foundation for Germline-Soma Communication. Curr Biol. 2018; 28(7):1124–1131.e3. [PubMed: 29576478]

Eppig JJ. Reproduction: Oocytes Call, Granulosa Cells Connect. Curr Biol. 2018; 28(8):R354–r356. [PubMed: 29689210]

Ernst EH, Franks S, Hardy K, Villesen P, Lykke-Hartmann K. Granulosa cells from human primordial and primary follicles show differential gene expression profiles. Hum Reprod. 2018a; 33(4):666–679. [PubMed: 29506120]

Ernst EH, Franks S, Hardy K, Villesen P, Lykke-Hartmann K. Granulosa cells from human primordial and primary follicles show differential global gene expression profiles. Hum Reprod. 2018b; 33(4):666–679. [PubMed: 29506120]

Ford E, Beckett EL, Roman S, McLaughlin EA, Sutherland J. Advances in human primordial follicle activation and premature ovarian insufficiency. Reproduction. 2019

Gougeon A. Regulation of ovarian follicular development in primates: facts and hypotheses. Endocr Rev. 1996; 17(2):121–55. [PubMed: 8706629]

Gowin K, Kosiorek H, Dueck A, Mascarenhas J, Hoffman R, Reeder C, Camoriano J, Tibes R, Gano K, Palmer J, Mesa R. Multicenter phase 2 study of combination therapy with ruxolitinib and danazol in patients with myelofibrosis. Leuk Res. 2017; 60:31–31. [PubMed: 28646676]

Gual P, Baron V, Lequoy V, Van Obberghen E. Interaction of Janus kinases JAK-1 and JAK-2 with the insulin receptor and the insulin-like growth factor-1 receptor. Endocrinology. 1998; 139(3):884–93. [PubMed: 9492017]

Hall SE, Upton RMO, McLaughlin EA, Sutherland JM. Phosphoinositide 3-kinase/protein kinase B (PI3K/AKT) and Janus kinase/signal transducer and activator of transcription (JAK/STAT) follicular signalling is conserved in the mare ovary. Reprod Fertil Dev. 2017

Hirahara K, Onodera A, Villarino Alejandro V, Bonelli M, Sciumè G, Laurence A, Sun H-W, Brooks Stephen R, Vahedi G, Shih H-Y, Gutierrez-Cruz G, et al. Asymmetric Action of STAT Transcription Factors Drives Transcriptional Outputs and Cytokine Specificity. Immunity. 2015; 42(5):877–889. [PubMed: 25992861]

Hsueh AJ, Kawamura K, Cheng Y, Fauser BC. Intraovarian control of early folliculogenesis. Endocr Rev. 2015; 36(1):1–24. [PubMed: 25202833]
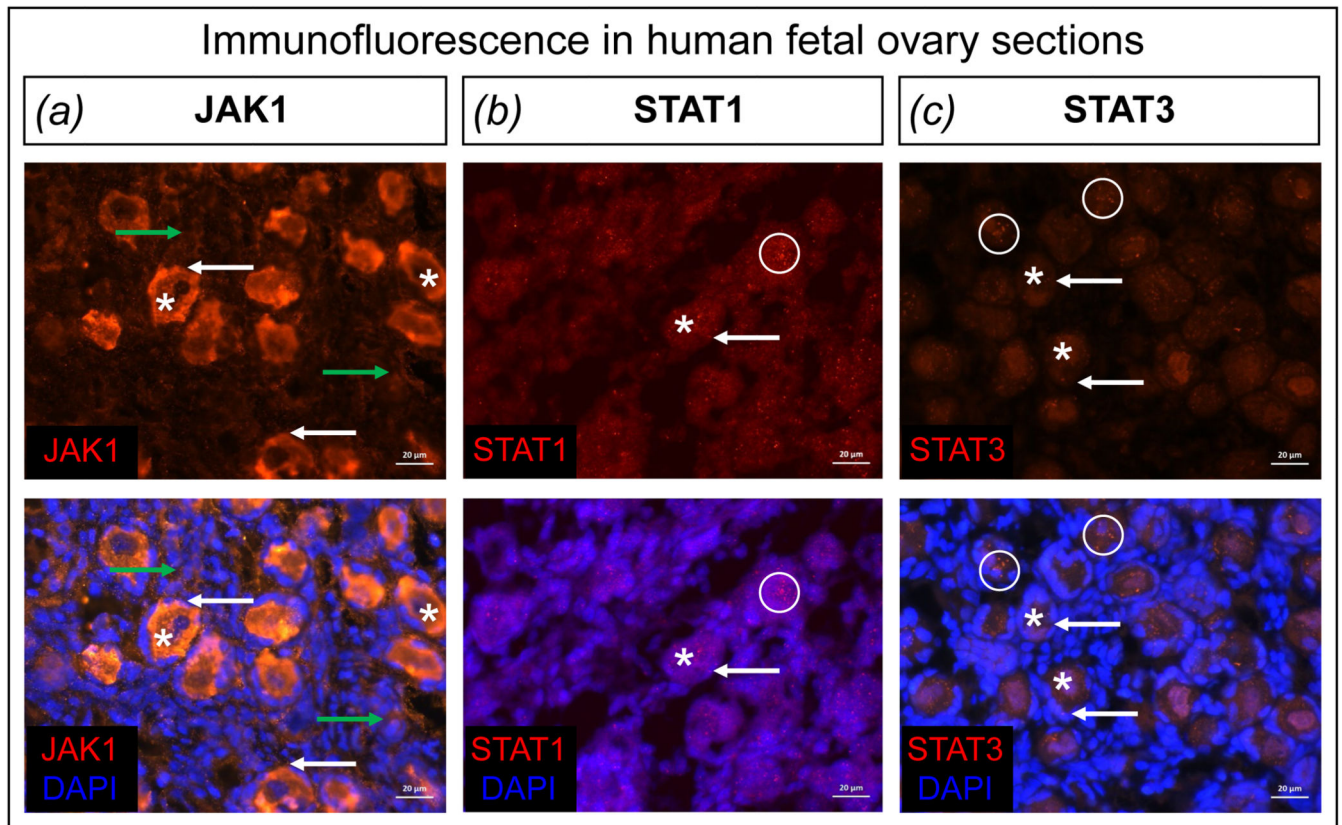
Huang K, Wang Y, Zhang T, He M, Sun G, Wen J, Yan H, Cai H, Yong C, Xia G, Wang C. JAK signaling regulates germline cyst breakdown and primordial follicle formation in mice. Biology Open. 2018; 7(1)

Inhorn MC, Patrizio P. Infertility around the globe: new thinking on gender, reproductive technologies and global movements in the 21st century. Human Reproduction Update. 2015; 21(4):411–426. [PubMed: 25801630]

Jia H, Song L, Cong Q, Wang J, Xu H, Chu Y, Li Q, Zhang Y, Zou X, Zhang C, Chin YE, et al. The LIM protein AJUBA promotes colorectal cancer cell survival through suppression of JAK1/ STAT1/IFIT2 network. Oncogene. 2017; 36(19):2655–2666. [PubMed: 27893714]

Kallen A, Polotsky AJ, Johnson J. Untapped Reserves: Controlling Primordial Follicle Growth Activation. Trends Mol Med. 2018; 24(3):319–331. [PubMed: 29452791]

Khan R, Lee JE, Yang YM, Liang FX, Sehgal PB. Live-cell imaging of the association of STAT6-GFP with mitochondria. PLoS One. 2013; 8(1):e55426. [PubMed: 23383189]

Kisseleva T, Bhattacharya S, Braunstein J, Schindler C. Signaling through the JAK/STAT pathway, recent advances and future challenges. Gene. 2002; 285(1):1–24. [PubMed: 12039028]

Kuepper MK, Butow M, Herrmann O, Ziemons J, Chatain N, Maurer A, Kirschner M, Maie T, Costa IG, Eschweiler J, Koschmieder S, et al. Stem cell persistence in CML is mediated by extrinsically activated JAK1-STAT3 signaling. Leukemia. 2019; 33(8):1964–1977. [PubMed: 30842608]

Kumar A, Commane M, Flickinger TW, Horvath CM, Stark GR. Defective TNF-α-Induced Apoptosis in STAT1-Null Cells Due to Low Constitutive Levels of Caspases. Science. 1997; 278(5343):1630–1632. [PubMed: 9374464]

Laissue P, Vinci G, Veitia RA, Fellous M. Recent advances in the study of genes involved in non-syndromic premature ovarian failure. Mol Cell Endocrinol. 2008; 282(1-2):101–11. [PubMed: 18164539]

Liang YB, Tang H, Chen ZB, Zeng LJ, Wu JG, Yang W, Li ZY, Ma ZF. Downregulated SOCS1 expression activates the JAK1/STAT1 pathway and promotes polarization of macrophages into M1 type. Mol Med Rep. 2017; 16(5):6405–6411. [PubMed: 28901399]

Lobie PE, Wood TJ, Chen CM, Waters MJ, Norstedt G. Nuclear translocation and anchorage of the growth hormone receptor. J Biol Chem. 1994; 269(50):31735–46. [PubMed: 7989347]

McLaughlin EA, McIver SC. Awakening the oocyte: controlling primordial follicle development. Reproduction. 2009; 137(1):1–11. [PubMed: 18827065]

Monahan AJ, Starz-Gaiano M. Socs36E attenuates STAT signaling to optimize motile cell specification in the Drosophila ovary. Dev Biol. 2013; 379(2):152–66. [PubMed: 23583584]

Norris RP, Freudzon M, Mehlmann LM, Cowan AE, Simon AM, Paul DL, Lampe PD, Jaffe LA. Luteinizing hormone causes MAP kinase-dependent phosphorylation and closure of connexin 43 gap junctions in mouse ovarian follicles: one of two paths to meiotic resumption. Development. 2008; 135(19):3229–38. [PubMed: 18776144]

Pastuschek J, Poetzsch J, Morales-Prieto DM, Schleussner E, Markert UR, Georgiev G. Stimulation of the JAK/STAT pathway by LIF and OSM in the human granulosa cell line COV434. J Reprod Immunol. 2015; 108:48–48. [PubMed: 25817464]

Peng M, Wang Y, Qiang L, Xu Y, Li C, Li T, Zhou X, Xiao M, Wang J. Interleukin-35 Inhibits TNF-alpha-Induced Osteoclastogenesis and Promotes Apoptosis via Shifting the Activation From TNF Receptor-Associated Death Domain (TRADD)-TRAF2 to TRADD-Fas-Associated Death Domain by JAK1/STAT1. Front Immunol. 2018; 9:1417. [PubMed: 30061878]

Quintas-Cardama A, Vaddi K, Liu P, Manshouri T, Li J, Scherle PA, Caulder E, Wen X, Li Y, Waeltz P, Rupar M, et al. Preclinical characterization of the selective JAK1/2 inhibitor INCB018424: therapeutic implications for the treatment of myeloproliferative neoplasms. Blood. 2010; 115(15):3109–17. [PubMed: 20130243]

Radler PD, Wehde BL, Wagner KU. Crosstalk between STAT5 activation and PI3K/AKT functions in normal and transformed mammary epithelial cells. Mol Cell Endocrinol. 2017; 451:31–31. [PubMed: 28495456]

Rajareddy S, Reddy P, Du C, Liu L, Jagarlamudi K, Tang W, Shen Y, Berthet C, Peng SL, Kaldis P, Liu K. p27kip1 (cyclin-dependent kinase inhibitor 1B) controls ovarian development by

suppressing follicle endowment and activation and promoting follicle atresia in mice. Mol Endocrinol. 2007; 21(9):2189–202. [PubMed: 17565040]

Rotgers E, Jorgensen A, Yao HH. At the Crossroads of Fate-Somatic Cell Lineage Specification in the Fetal Gonad. Endocr Rev. 2018; 39(5):739–759. [PubMed: 29771299]

Sadzak I, Schiff M, Gattermeier I, Glinitzer R, Sauer I, Saalmüller A, Yang E, Schaljo B, Kovarik P. Recruitment of Stat1 to chromatin is required for interferon-induced serine phosphorylation of Stat1 transactivation domain. Proceedings of the National Academy of Sciences. 2008; 105(26):8944–8949.

Sakamoto K, Wehde BL, Yoo KH, Kim T, Rajbhandari N, Shin HY, Triplett AA, Radler PD, Schuler F, Villunger A, Kang K, et al. Janus Kinase 1 Is Essential for Inflammatory Cytokine Signaling and Mammary Gland Remodeling. Mol Cell Biol. 2016; 36(11):1673–90. [PubMed: 27044867]

Sanda T, Tyner JW, Gutierrez A, Ngo VN, Glover J, Chang BH, Yost A, Ma W, Fleischman AG, Zhou W, Yang Y, et al. TYK2-STAT1-BCL2 pathway dependence in T-cell acute lymphoblastic leukemia. Cancer discovery. 2013; 3(5):564–577. [PubMed: 23471820]

Schiavone D, Avalle L, Dewilde S, Poli V. The immediate early genes Fos and Egr1 become STAT1 transcriptional targets in the absence of STAT3. FEBS Letters. 2011; 585(15):2455–2460. [PubMed: 21723864]

Shaker ME, Hazem SH, Ashamallah SA. Inhibition of the JAK/STAT pathway by ruxolitinib ameliorates thioacetamide-induced hepatotoxicity. Food Chem Toxicol. 2016; 96:290–290. [PubMed: 27546300]

Shelling AN. Premature ovarian failure. Reproduction. 2010; 140(5):633–41. [PubMed: 20716613]

Sobinoff AP, Beckett EL, Jarnicki AG, Sutherland JM, McCluskey A, Hansbro PM, McLaughlin EA. Scrambled and fried: cigarette smoke exposure causes antral follicle destruction and oocyte dysfunction through oxidative stress. Toxicol Appl Pharmacol. 2013; 271(2):156–67. [PubMed: 23693141]

Sutherland JM, Frost ER, Ford EA, Peters AE, Reed NL, Seldon AN, Mihalas BP, Russel DL, Dunning KR, McLaughlin EA. Janus Kinase JAK1 maintains the ovarian reserve of primordial follicles in the mouse ovary. Mol Hum Reprod. 2018

Sutherland JM, Keightley RA, Nixon B, Roman SD, Robker RL, Russell DL, McLaughlin EA. Suppressor of cytokine signaling 4 (SOCS4): moderator of ovarian primordial follicle activation. J Cell Physiol. 2012; 227(3):1188–98. [PubMed: 21604262]

van den Berg-Bakker CA, Hagemeijer A, Franken-Postma EM, Smit VT, Kuppen PJ, van Ravenswaay Claasen HH, Cornelisse CJ, Schrier PI. Establishment and characterization of 7 ovarian carcinoma cell lines and one granulosa tumor cell line: growth features and cytogenetics. Int J Cancer. 1993; 53(4):613–20. [PubMed: 8436435]

Verstovsek S, Gotlib J, Mesa RA, Vannucchi AM, Kiladjian JJ, Cervantes F, Harrison CN, Paquette R, Sun W, Naim A, Langmuir P, et al. Long-term survival in patients treated with ruxolitinib for myelofibrosis: COMFORT-I and -II pooled analyses. J Hematol Oncol. 2017; 10(1):156. [PubMed: 28962635]

Wang S, Raven JF, Durbin JE, Koromilas AE. Stat1 phosphorylation determines Ras oncogenicity by regulating p27 kip1. PloS one. 2008; 3(10):e3476–e3476. [PubMed: 18941537]

Wang S, Raven JF, Koromilas AE. STAT1 represses Skp2 gene transcription to promote p27Kip1 stabilization in Ras-transformed cells. Mol Cancer Res. 2010; 8(5):798–805. [PubMed: 20407011]

Wang S, Zhang X, Wang G, Cao B, Yang H, Jin L, Cui M, Mao Y. Syndecan-1 suppresses cell growth and migration via blocking JAK1/STAT3 and Ras/Raf/MEK/ERK pathways in human colorectal carcinoma cells. BMC Cancer. 2019; 19(1):1160. [PubMed: 31783811]

Wei Z, Jiang X, Qiao H, Zhai B, Zhang L, Zhang Q, Wu Y, Jiang H, Sun X. STAT3 interacts with Skp2/p27/p21 pathway to regulate the motility and invasion of gastric cancer cells. Cell Signal. 2013; 25(4):931–8. [PubMed: 23333463]

Xiong Y, Liu T, Wang S, Chi H, Chen C, Zheng J. Cyclophosphamide promotes the proliferation inhibition of mouse ovarian granulosa cells and premature ovarian failure by activating the lncRNA-Meg3-p53-p66Shc pathway. Gene. 2017; 596:1–1. [PubMed: 27729272]

Yang MY, Fortune JE. Changes in the transcriptome of bovine ovarian cortex during follicle activation in vitro. Physiol Genomics. 2015; 47(12):600–11. [PubMed: 26443523]

Zhang H, Risal S, Gorre N, Busayavalasa K, Li X, Shen Y, Bosbach B, Brannstrom M, Liu K. Somatic cells initiate primordial follicle activation and govern the development of dormant oocytes in mice. Curr Biol. 2014; 24(21):2501–8. [PubMed: 25438940]

Zhang H, Vollmer M, De Geyter M, Litzistorf Y, Ladewig A, Durrenberger M, Guggenheim R, Miny P, Holzgreve W, De Geyter C. Characterization of an immortalized human granulosa cell line (COV434). Mol Hum Reprod. 2000; 6(2):146–53. [PubMed: 10655456]

Zhang Y, Yan Z, Qin Q, Nisenblat V, Chang HM, Yu Y, Wang T, Lu C, Yang M, Yang S, Yao Y, et al. Transcriptome Landscape of Human Folliculogenesis Reveals Oocyte and Granulosa Cell Interactions. Mol Cell. 2018; 72(6):1021–1034.e4. [PubMed: 30472193]

Zouein FA, Duhe RJ, Booz GW. JAKs go nuclear: emerging role of nuclear JAK1 and JAK2 in gene expression and cell growth. Growth Factors. 2011; 29(6):245–52. [PubMed: 21892841]

Summary text

The development of a healthy oocyte within the ovary is critical for human fertility. This study found that members of the JAK/STAT signalling pathway are expressed in the human ovary, specifically in the cells that support oocyte development. These results highlight the need for a greater understanding of ovarian signalling and what the consequences are for female fertility.

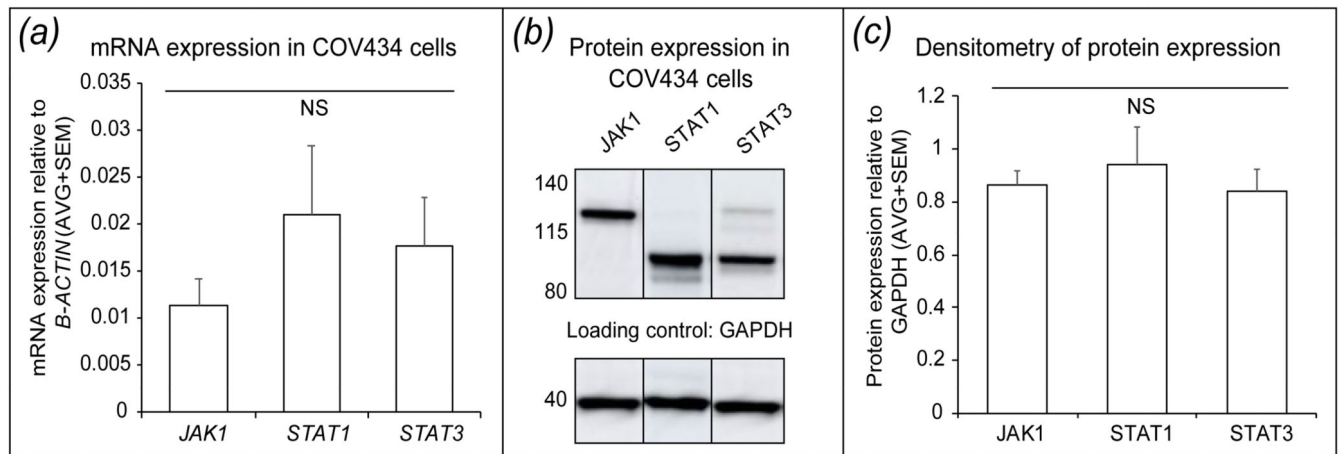**Figure 1. Protein localisation of JAK1, STAT1 and STAT3 in human foetal ovarian sections**

Representative protein localisation was analysed using immunofluorescence for JAK1, STAT1 and STAT3 in human foetal ovarian sections (Figure 1*a*, 1*b* and 1*c*). JAK1 and STAT3 protein was expressed in both the oocyte (white asterisks) and the granulosa cells (white arrows) of primordial follicles. JAK1 was faintly detected in the stromal and interstitial cells of the foetal ovary (identified by green arrows). STAT1 showed weak protein expression in the surrounding granulosa cells, however distinct STAT1 foci were detected in the nucleus of oocytes (identified by white circles in Figure 1*b*). Aggregates of STAT3 protein were observed in the nucleus of the oocytes (identified by white circles in Figure 1*c*). All sections were counter-stained with DAPI (blue). Scale bar in all images is 20 μm.

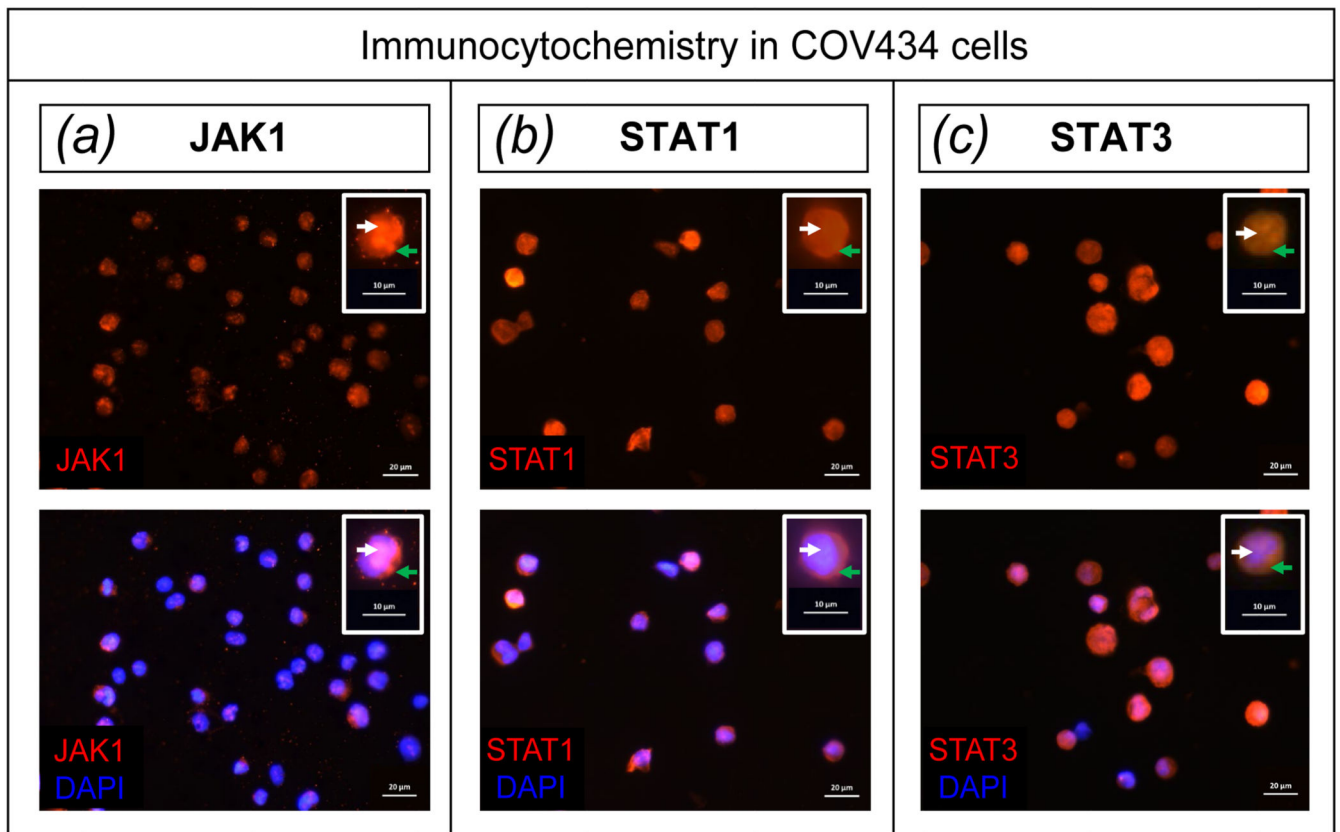**Figure 2. Protein localisation of JAK1, STAT1 and STAT3 in human pre-menopausal ovarian sections**

Representative protein localisation was analysed using immunofluorescence for JAK1, STAT1 and STAT3 in human pre-menopausal ovarian sections (Figure 2*a*, 2*b* and 2*c*). Both primordial and primary follicles were identified in the ovary sections (according to Gougeon's criteria (Gougeon 1996)). JAK1 showed protein expression in both the oocyte (white asterisks) and the granulosa cells (white arrows) of primordial follicles (Figure 2*a*). In primary follicles, however, JAK1 was restricted to the granulosa cells, and was undetectable in the oocyte (Figure 2*a*). STAT1 showed weak protein expression in the

oocyte and surrounding granulosa cells (Figure 2*b*). Aggregates of STAT1 protein were observed in the nucleus of the oocytes (identified by white circles in Figure 2*b*). STAT3 protein was intensely localised to the pre-granulosa and granulosa cells of both follicle types (Figure 2*c*). All sections were counter-stained with DAPI (blue). Scale bar in all images is 20 μm.

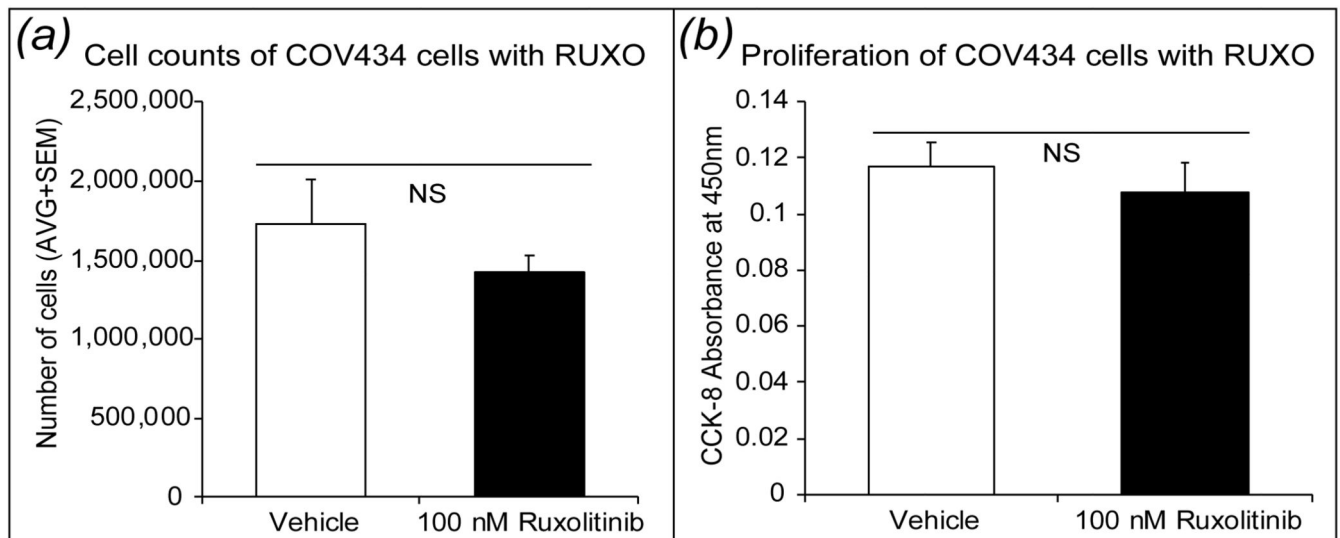**Figure 3. Expression of JAK/STAT members in COV434 cells**

Relative mRNA expression levels of *JAK1, STAT1* and *STAT3* in COV434 cells (Figure 3*a*). Data was normalised to the house-keeping gene *B-ACTIN* and is presented as mean ± SEM (n = 4). No changes in mRNA expression were observed between genes. Relative protein expression levels in COV434 cells for JAK1, STAT1 and STAT3, with representative blots (Figure 3*b*) and the corresponding densitometry analysis (Figure 3*c*). The density of each protein band was quantified relative to the GAPDH immunoblots, with no significant differences and is plotted as the mean ± SEM (n = 4). NS indicates no statistical significance.
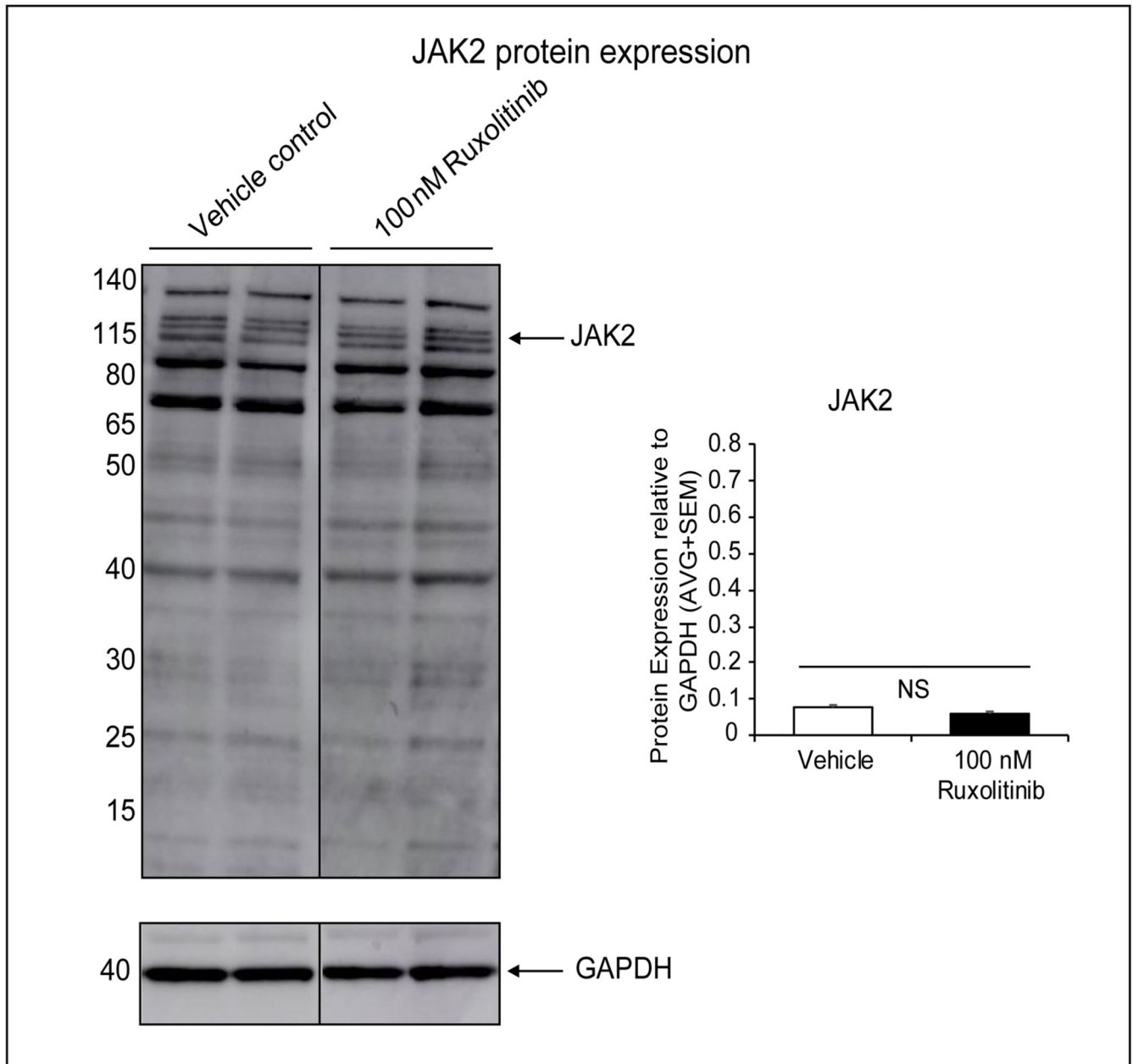
Figure 4. Protein localisation of JAK/STAT members in COV434 cells

Representative protein localisation was analysed for JAK1 (Figure 4*a*), STAT1 (Figure 4*b*) and STAT3 (Figure 4*c*). Nuclear and cytoplasmic expression was seen for JAK1, STAT1 and STAT3. In the insert images, white arrowheads label the nucleus of cells, and the green arrowheads label the cytoplasm of cells. The scale bar in larger images is 20 μm, and in the insert images, the scale bar is 10 μm.
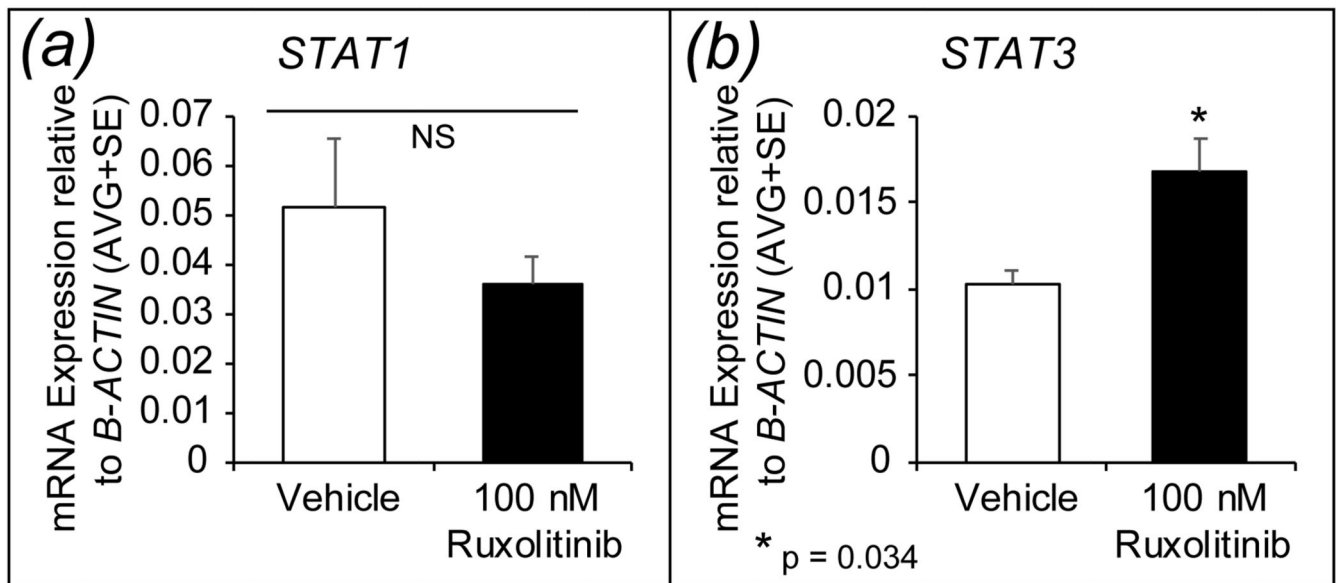
Figure 5. Effects of Ruxolitinib treatment on COV434 cell death and proliferation dynamics
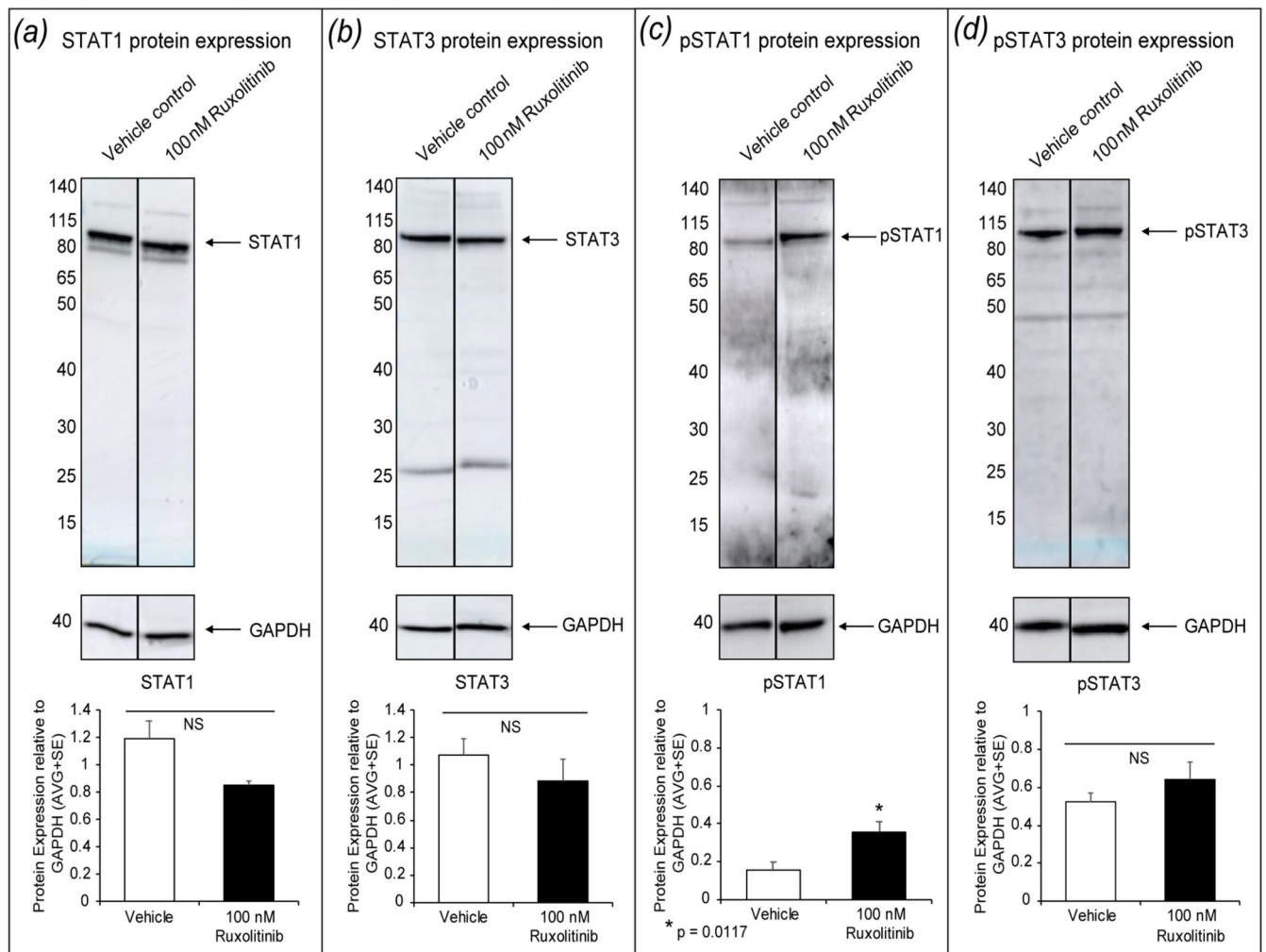
Cell counts of COV434 cells following 72 h treatment with 100 nM Ruxolitinib or vehicle control (Figure 5*a*). No significant difference in cell number between the two treatment groups was observed and data is plotted as the mean ± SEM (n = 4). Cell counting kit-8 (CCK-8) absorbance values were used as a measure of proliferation in COV434 cells (Figure 5*b*). COV434 cells were treated for 72 h with 100 nM Ruxolitinib or vehicle control. No significant difference in absorbance values was observed between the treatment groups. Data is presented as the mean ± SEM (n = 8) and NS indicates no statistical significance.

Figure 6. Protein expression of JAK2 in COV434 cells following Ruxolitinib treatment
JAK2 protein expression is shown with representative blots and the corresponding densitometry analysis below (Figure 6). JAK2 protein expression levels in COV434 cells treated with 100 nM Ruxolitinib (black bars) or vehicle control (white bars) are shown in the densitometry graph. The density of each protein band was quantified relative to the GAPDH immunoblots and is plotted as mean ± SEM (n = 4). NS indicates no statistical significance.
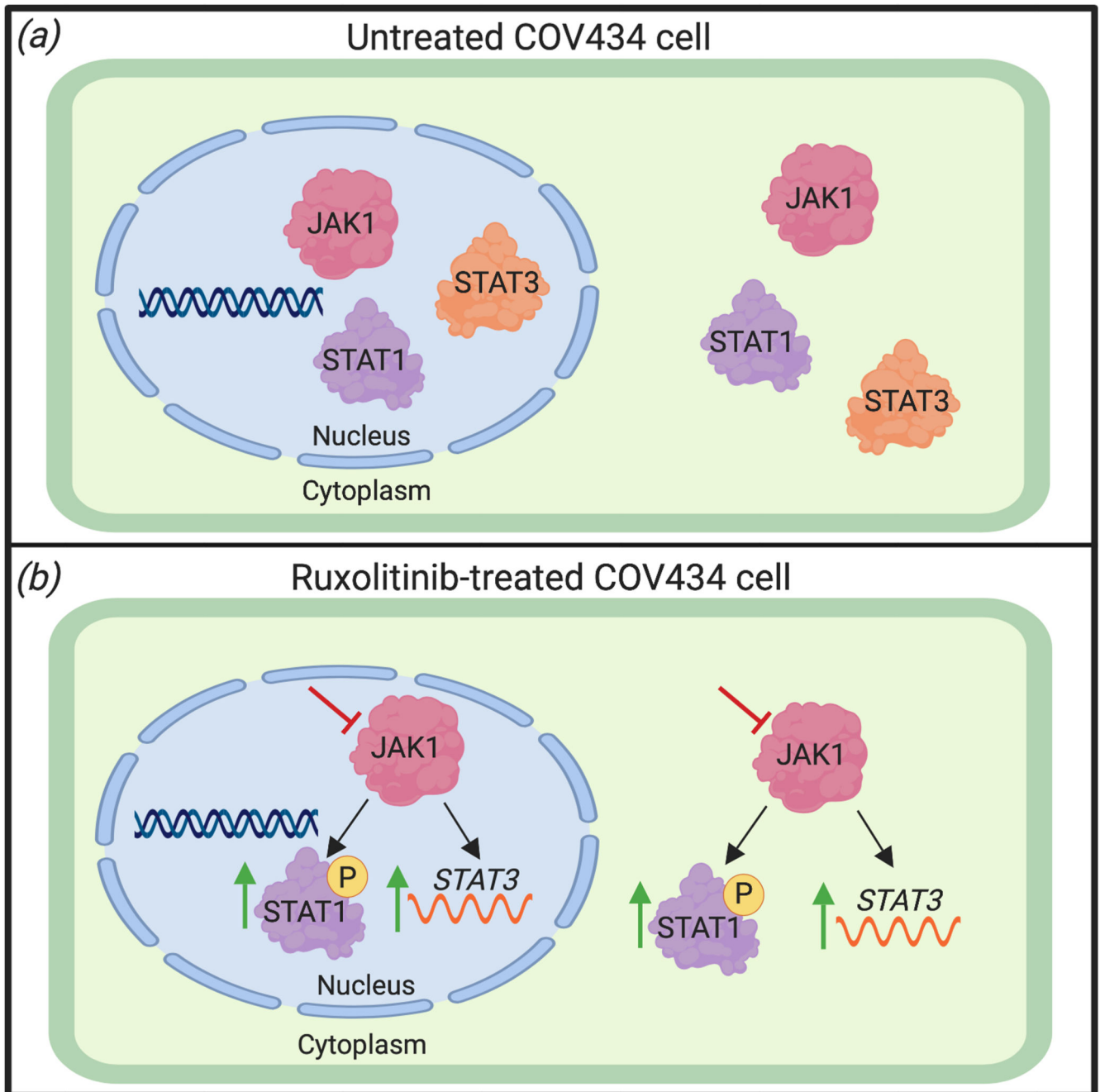
Figure 7. Expression of STAT1 and STAT3 mRNA in COV434 cells with Ruxolitinib treatment
COV434 cells were treated for 72 h with 100 nM Ruxolitinib (black bars) or vehicle control
(white bars). The relative mRNA expression levels of *STAT1* (Figure 7*a*) and *STAT3*
(Figure 7*b*) are shown. *STAT3* mRNA increased significantly with Ruxolitinib treatment (p
= 0.034). Data was normalised to the house-keeping gene *B-ACTIN* and is presented as the
mean ± SEM (n = 4). Asterisk (*) indicates p   0.05 and NS shows no statistical
significance.

Figure 8. Effects of Ruxolitinib treatment on STAT protein expression in COV434 cells

COV434 cells were treated for 72h with 100 nM Ruxolitinib (black bars) or vehicle control (white bars). Cells were collected following treatment for total protein analysis. The relative protein expression levels in treated COV434 cells for STAT1 (Figure 8*a*), STAT3 (Figure 8*b*), phosphorylated Y701 STAT1 (Figure 8*c*) and phosphorylated Y705 STAT3 (Figure 8*d*) are shown. Protein expression is shown with representative blots and the corresponding densitometry analysis below. A significant increase in pSTAT1 protein was found with Ruxolitinib treatment (p = 0.0025). For STAT1 and STAT3 blots, the density of each protein band was quantified relative to the GAPDH immunoblots and is plotted as mean ± SEM (n = 4). For pSTAT1 and pSTAT3 blots, the density of each protein band was quantified relative to the GAPDH immunoblots and is plotted as mean ± SEM (n = 7). Asterisk (*) indicates p 0.05 and NS shows no statistical significance.

Figure 9. Summary of the effect of JAK1 inhibition on STAT signalling in COV434 cells
In untreated COV434 cells, JAK1, STAT1 and STAT3 proteins are expressed in both the
nucleus and the cytoplasm of the cell (Figure 9*a*). In cells treated with the JAK1-inhibitor
Ruxolitinib, JAK1 protein is inhibited. This leads to an increase of *STAT3* mRNA and
phosphorylated STAT1 protein within the cell (Figure 9*b*). Figure 9 was created with
BioRender.com.

Table I

Primer sequences for real-time PCR

Name		Primer Sequence	Annealing Temperature (°C)	Efficiency in COV434 cells
JAK1	Forward	AGACTTGTGAATACGTTAAAAGAAGGA	59	2.03
	Reverse	AAAGCTTGTCCGATTGGATG		
STAT1	Forward	CTTACCCAGAATGCCCTGAT	65	1.78
	Reverse	CGAACTTGCTGCAGACTCTC		
STAT3	Forward	GGTCTGGCTGGACAATATCATT	65	1.87
	Reverse	GAGGCTTAGTGCTCAAGATGG		
B-ACTIN	Forward	TGTGGCATCCACGAAACTACC	65	1.96
	Reverse	ACATCTGCTGGAAGGTGGACA		

Table II

Immunofluroescence results showing relative expression of candidate proteins in COV434 cells

Name	Cell compartment	Relative expression (Immunofluroescence)
JAK1	Nucleus	High expression
	Cytoplasm	Medium expression
STAT1	Nucleus	High expression
	Cytoplasm	High expression
STAT3	Nucleus	Medium expression
	Cytoplasm	Medium expression